Nanostructure Evolution of Isotropic High-Pressure Injection-Molded UHMWPE during Heating

4 AUTHORS, INCLUDING:

Benjamin S Hsiao
Stony Brook University
572 PUBLICATIONS   20,609 CITATIONS

SEE PROFILE

Rainer Gehrke
Deutsches Elektronen-Synchrotron
170 PUBLICATIONS   1,573 CITATIONS

SEE PROFILE

Nanostructure Evolution of Isotropic High-Pressure Injection-Molded UHMWPE during Heating

Zhi-Gang Wang,[†] Benjamin S. Hsiao,[†] Norbert Stribeck,*,[‡] and Rainer Gehrke[§]

Department of Chemistry, State University of New York at Stony Brook, Stony Brook, New York 11794-3400; Institut für Technische und Makromolekulare Chemie, Universität Hamburg, 20146 Hamburg, Germany; and HASYLAB at DESY, Notkestrasse 85, 22603 Hamburg, Germany

ABSTRACT: Ultrahigh molecular weight polyethylene (UHMWPE) is injection molded under high pressure and studied by ultra-small-angle X-ray scattering (USAXS) during melting in a time-resolved synchrotron radiation experiment. Results concerning melting and recrystallization of crystalline lamellae are compared to data obtained by differential scanning calorimetry (DSC). USAXS analysis reveals a coupled process of melting and crystallization which is not accompanied by external heat flow. Nine isotropic samples differing in molecular weight and molding pressure are heated at a rate of 5 °C/min. 2D USAXS images integrate over temperature intervals between 3 and 7 °C. The materials are considered two-phase semicrystalline polymers. Scattering curves obtained by azimuthal averaging are transformed to interface distribution functions (IDF) which are perfectly fitted by a nanostructural model comprising an ensemble of thick, uncorrelated layers (50 nm thickness) and stacks of short-range correlated crystalline lamellae (20 nm). Crystalline layers are identified from their narrower layer thickness distribution and their melting behavior. After the scattering effect of amorphous layers is eliminated, a composite crystallite thickness distribution is obtained. Its variation is studied as a function of temperature, molecular mass and molding pressure. In DSC thermograms samples prepared at high pressure exhibit a single strong melting peak, whereas the other samples show an additional melting peak at lower temperature. This might lead to the conclusion that the high-pressure samples predominantly contain extended chain crystals. USAXS shows that high-pressure materials contain considerable amounts of imperfect thin crystal lamellae that melt at lower temperature, while thick lamellae are formed. With low-pressure samples, this coupled process of nanostructure transformation during annealing is found to be negligible.

Introduction

Melting and crystallization of polyethylene (PE) and ultra-high-molecular-weight polyethylene (UHMWPE) has been the subject of numerous studies for several decades. Although crystallization and melting data for polyethylene is extremely rich, structural information on the corresponding processes is rare and incomplete.[1] To follow the rapid and subtle changes of the two-phase nanostructure of high-pressure injection-molded UH-MWPE we have adopted the method of ultra-small-angle X-ray scattering (USAXS) with synchrotron radiation.

More and more Ruland's IDF method[2] is utilized to extract the information on the ideal lamellar two-phase system from such scattering data. Subsequently, the resulting "interface distribution function" is interpreted or analyzed.[3−21] Strobl, in particular, has drawn some interesting conclusions concerning the process of crystallization from a combination of IDF interpretation[22] and electron microscopic method.[23] In this article, we apply a recently proposed method for the automated extraction of the IDF[24] to a big number of scattering patterns, analyze the nanostructure by fitting of an adapted model for the lamellar two-phase system, and compare the results to the information of DSC thermograms.

Materials were prepared under high pressure in such a way that a transition from solidification[25] crystallized lamellae to the extended-chain lamellae should be observed, which first were reported by Wunderlich[26] and have remained a vivid field of research since.
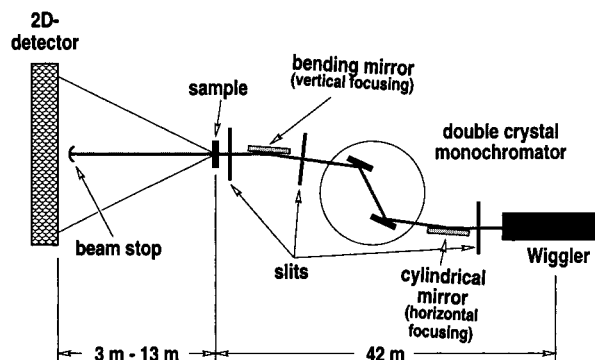
[†] State University of New York at Stony Brook.
[‡] Universität Hamburg.
[§] HASYLAB at DESY.

Figure 1. Sketch of the optics of the BW4 USAXS beamline at HASYLAB, Hamburg, Germany.

Experimental Section

Three grades of ultrahigh molecular weight polyethylene (UHMWPE, Hoechst-Celanese Inc.) of different molecular mass were investigated ($M_w/(10^6$ g/mol) = 4, 5, 6). From the supplied powders rods were injection molded at three different pressures (p = 210, 240, 280 MPa) using a modified capillary rheometer. The materials were equilibrated in the molten state (252 °C) for 5 min and then pressurized for 30 min. Thereafter the rods were recovered by cooling the samples at a rate of about 1 °C/min under an isobaric condition. For the USAXS measurements, disks with a diameter of 8 mm and a thickness of 2 mm were wrapped in aluminum foil and fixed in a copper sample frame. After the melting/crystallization cycle, the shape of the samples had not changed.

Ultra-small-angle X-ray scattering (USAXS) was performed in the synchrotron beam line BW4 at HASYLAB, Hamburg, Germany (cf. Figure 1). The wavelength of the X-ray beam was 0.1366 nm. USAXS images were collected by a two-dimensional position sensitive Gabriel detector (512 × 512 pixels of 0.4 × 0.4 mm²) (from European Molecular Biological Labora-
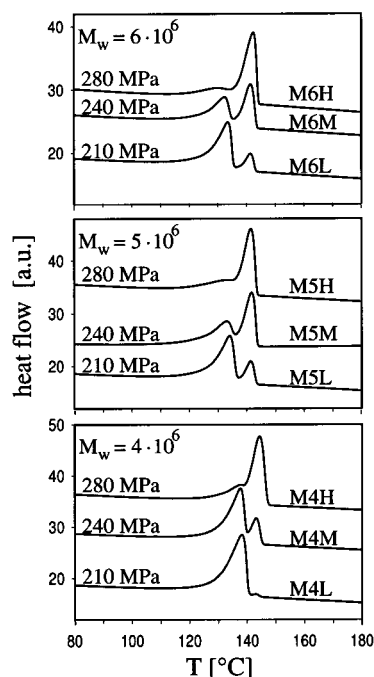
Figure 2. Melting of UHMWPE as a function of molecular mass and molding pressure studied by differential scanning calorimetry (DSC). Varied parameters are indicated on the left of each curve, sample denominations on the right.

tory, EMBL). The sample-to-detector distance was set to 12690 mm. The minimal accessible scattering angle corresponded to a *d* spacing of 860 nm. The maximal scattering angle corresponded to 16 nm. In the detector plane the beam was 0.5 mm high and 2 mm wide.

During image collection, each sample was heated from 25 to 250 °C at 5 °C/min. Images were accumulated for 90 s. Data storing took 30 s. So there is one image per 10 °C. Samples M6H and M4M (for sample denominations cf. Figure 2) were additionally heated at 6 °C/min up to 115 °C, slowed to 2 °C/min during the melting up to 145 °C, and speeded up to 6 °C/min again up to 250 °C. Thus, here, images were collected every 4 °C in the most interesting temperature range.

DSC scans were carried out in a Perkin-Elmer DSC-7 in a range from 25 to 180 °C with a heating rate of 5 °C/min.

DSC Results

DSC thermograms are shown in Figure 2. Characteristic parameters and sample designations used in the sequel are indicated in the figure. The samples exhibit two melting peaks. As a function of increasing molding pressure the low-temperature peak is decreasing, whereas the high-temperature peak becomes stronger. This finding is explained by "extended chain lamellae" formation by high-pressure crystallization, as was first reviewed by Wunderlich.[26] According to the DSC thermograms samples prepared at 280 GPa exhibit almost total conversion to extended chain lamellae which melt at temperature above 140 °C.

USAXS Data Evaluation

Extraction of the IDF. A total of 300 two-dimensional scattering patterns were normalized to detector efficiency and calibrated to incident beam flux and the irradiated volume. The slight anisotropy found with five of the samples was considered to be negligible. Background subtraction and sample absorption were subsequently performed. The sample absorption was determined experimentally at ambient temperature. Changes

during measurement were monitored using an ionization chamber in the beam stop. The center of the scattering pattern was determined and blind areas were masked in the images. From the remnant pixels in each image an azimuthal average scattering curve $I(s)$ was computed. $s = (2/\lambda) \sin \theta$ is defined by the wavelength of radiation, λ, and half the scattering angle, θ.

The lamellar two-phase nanostructure was analyzed by means of the interface distribution function (IDF), $g_1(x)$,[2] in which the nonideal character of the raw scattering is eliminated. Considering an ideal two-phase system the IDF represents the probability distribution of finding two interfaces (between a crystalline layer and the adjacent amorphous region) at a distance x from each other. The IDF is proportional to the second derivative of the one-dimensional correlation function, $\gamma_1(x)$.[27]

Computation of $g_1(x)$ was performed as follows. Bearing in mind Porod's law

$$I_P(s) = s^4(I(s) - c_{Fl})$$

was computed. The preliminary constant background, c_{Fl}, was determined by minimizing the function

$$T_c(c_{Fl}, A_p) = \sum_k (s_k^4(I_k - c_{Fl}) - A_P)^2 \qquad (1)$$

with the sum being extended over all measured data pairs (I_k, s_k) in the region where Porod's law was estimated to be valid ($0.045 \text{ nm}^{-1} < s < 0.06 \text{ nm}^{-1}$). If Porod's region is thus reasonably chosen, $I_P(s)$ receives an almost horizontal asymptote (cf. Figure 3). A_P specifies the asymptotic intensity falloff according to Porod's law. It shall be noted that this constant background subtraction is only a preparative step preceding the construction of a slowly varying background by the following spatial frequency filtering procedure. An unfavorable alternative is to perform spatial frequency filtering directly on the measured data. Compared to the chosen method this procedure leads to interference functions suffering from considerable damping of its oscillations.

In the next step, a slowly varying background was subtracted from $I_P(s)$ to obtain the interference function $G_1(s)$. As described recently[24,28] this background was generated from the scattering curve itself by low-pass spatial frequency filtering. One-dimensional Fourier transformation of $G_1(s)$ resulted in the IDF $g_1(x)$.

Choice of a Model for the Nanostructure. Several models were tested to fit the IDF data. As indicated by the complex shape of the scattering curves, a single stack proved insufficient. A double stack model resulted in perfect fits, but the width of one of the layer thickness distributions was found to be undefined. This finding showed that the corresponding component is pure particle scattering. In a next step the particle scattering was modeled by a skewed Gaussian thickness distribution as defined in earlier publications.[29,30] However, it turned out that this model was still too complex because regression output exhibited strong parameter–parameter correlations. After removal of a further parameter and assumption of pure Gaussian shape for the layer thickness distribution of the particle scattering, an adapted structural model was found. It yielded perfect fits with a small set of uncorrelated structural parameters (cf. Figure 4).
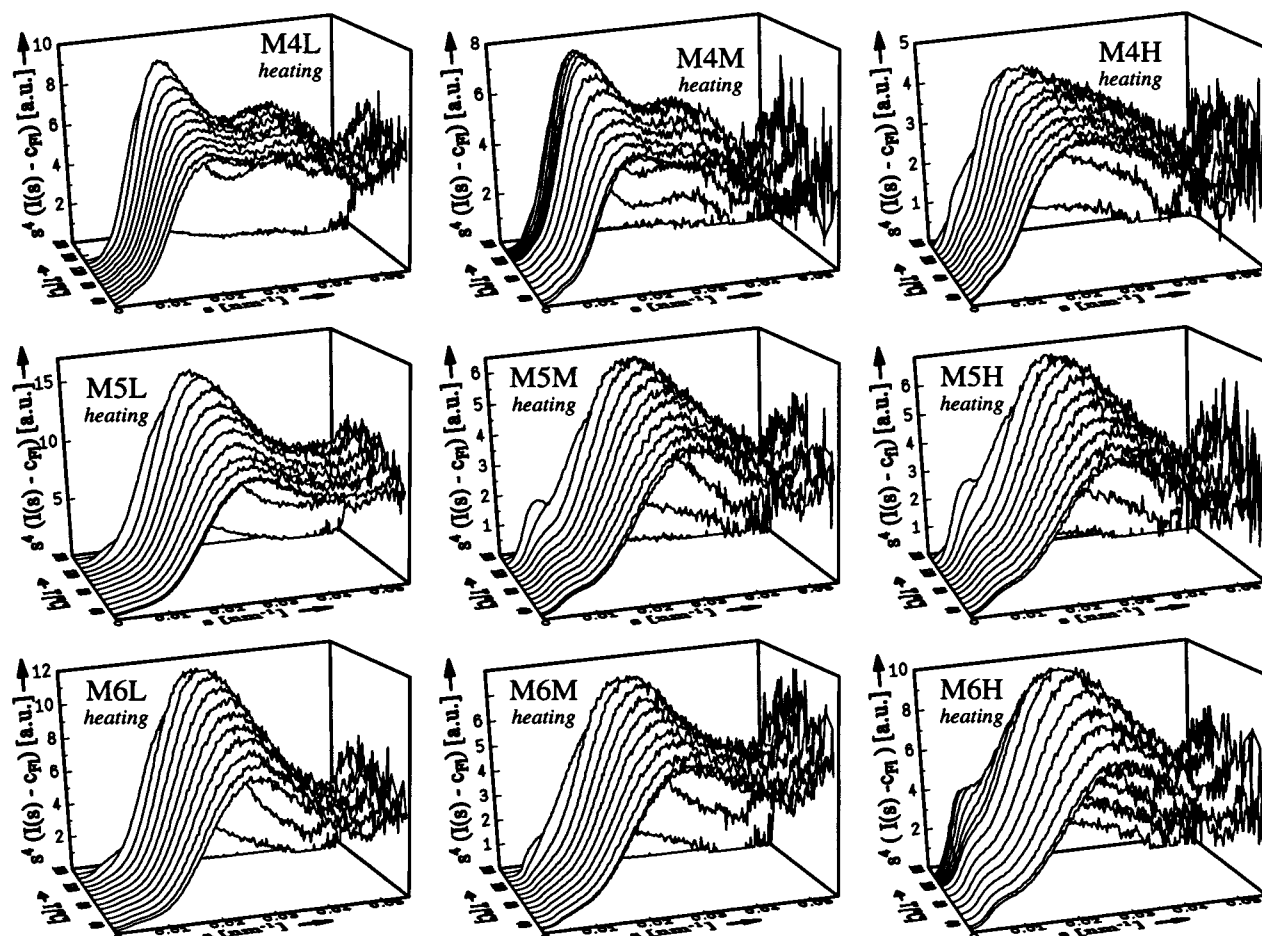
Figure 3. Melting of UHMWPE as a function of molecular mass and molding pressure. USAXS curves s^4 $(I(s) - c_{Fl})$ with c_{Fl} estimated from the tail of the curve. In all subfigures the s axis extends from left to right and comprises an interval 0 nm^{-1} < s < 0.055 nm^{-1}. The temperature axis extends from front to back and runs from 20 to 160 °C.
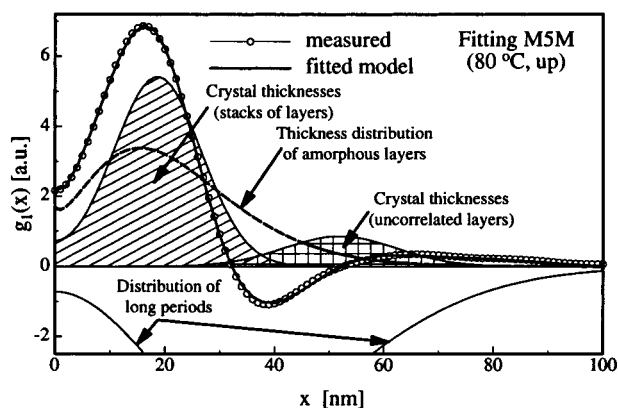

Figure 4. Demonstration of IDF fit by a model comprising an ensemble of uncorrelated crystalline lamellae (crosshatched layer thickness distribution) and stacked lamellae (hatched, crystal thickness distribution; dashed, amorphous thicknesses; below x axis, number distribution of long periods—going off-scale).

The layer stack component is described by six model parameters.[29] Three additional parameters describe particle scattering from uncorrelated lamellae, which was considered by a separate component to the scattering

$$2\pi s^2 I(s) = I_1(s) = \frac{W_p}{s^2} (1 - H_{c,p}(s)) \qquad (2)$$

with

$$H_{c,p}(s) = \cos(2\pi \bar{t}_{c,p} s)\exp(-2\pi^2 \sigma^2_{c,p} s^2)$$

The function $H_{c,p}(s)$ is the Fourier transform of the normalized layer thickness distribution, $h_{c,p}(x)$, and the quantity $W_p = 2\pi A_P$ is its weight. $\bar{t}_{c,p}$ is the average thickness of the uncorrelated crystalline layers and $\sigma_{c,p}^2$ the variance of the corresponding layer thickness distribution. Close to melting, pure particle scattering was observed with some of the samples, which could be fitted directly using eq 2.

Fractions of Crystalline Volume. The weights W_s and W_p of stack and particle components, respectively, are proportional to the product of the number of lamellae, their surfaces, and the square of the contrast. Because correlation among lamellae from the stacks is very low, contrast between amorphous density and crystalline density should be the same for correlated and uncorrelated lamellae (i.e. amorphous density inside the stack is assumed to be the same as amorphous density outside).

Then the fraction of crystalline volume organized in uncorrelated layers with respect to the total crystalline volume can be approximated by

$$V_{p,c} = \frac{\bar{t}_{c,p} W_p}{\bar{t}_{c,p} W_p + \bar{t}_{c,s} W_s} \qquad (3)$$
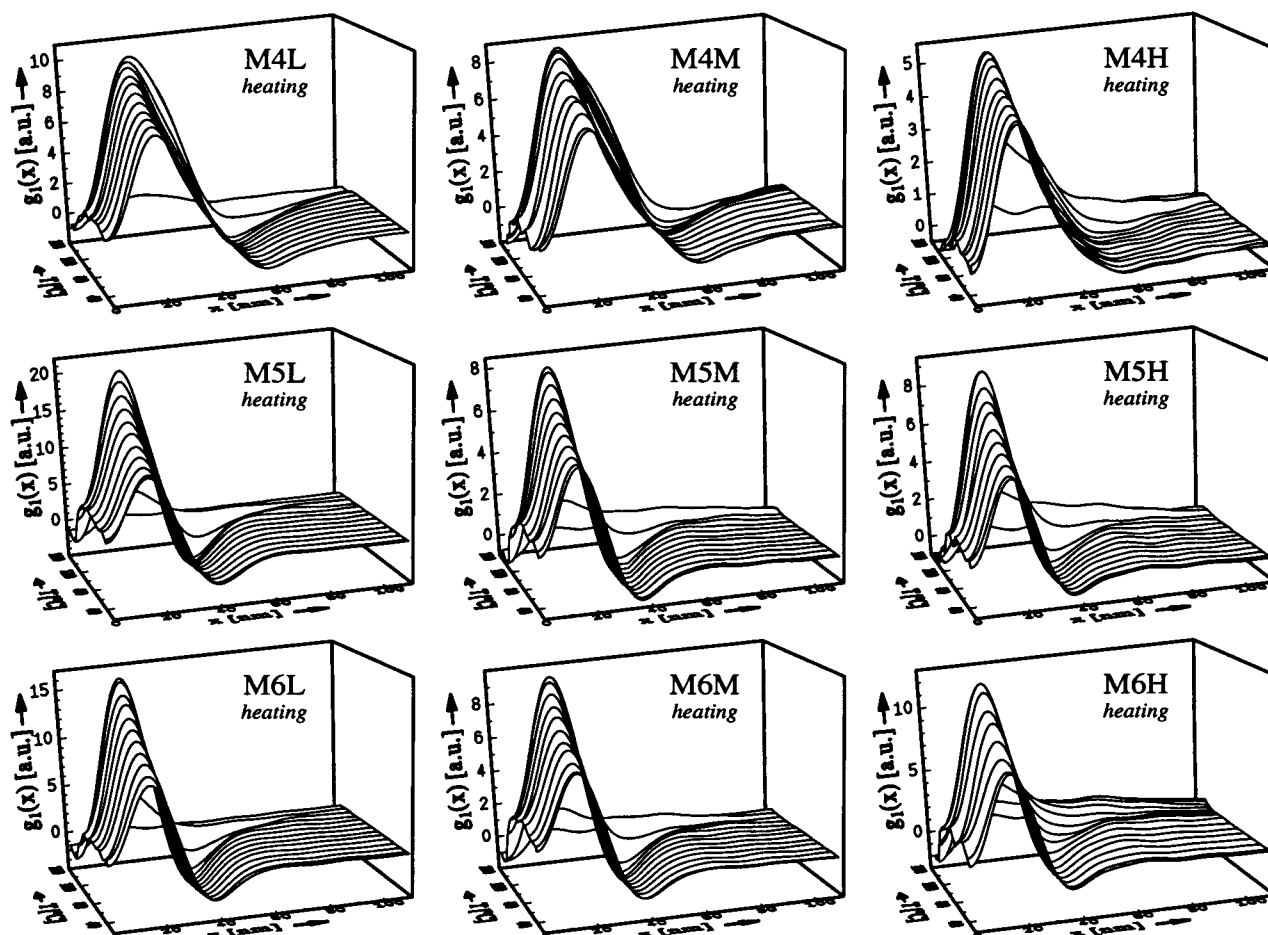
Figure 5. Interface distribution functions (IDFs) $g_1(x)$ computed from the scattering curves of UHMWPE as a function of molecular mass and molding pressure during heating and melting.

with $\bar{t}_{c,p}$ and $\bar{t}_{c,s}$ designating the average crystal thickness of the particles and the average crystal thickness inside the stacks, respectively.

During initial heating from room temperature the main effect on the observed USAXS is caused from contrast change. Thus, to a first approximation, contrast increase can be determined by linear extrapolation of the weight parameter $W(T)$ (cf. Figure 6) and eliminated from the weight of the crystal thickness distributions. Finally, after combining the two crystal thickness distributions (hatched areas in Figure 4) and multiplication by x, a function $xh_c(x)$ is obtained, which is proportional to the volume fraction in the sample filled by crystals of thickness x. It can be studied as a function of temperature and yields detailed in situ information on the melting and recrystallization of nanoscale lamellae during annealing and melting.

USAXS Results and Discussion

Figure 3 shows the scattering data in a representation emphasizing the scattering features of a domain structure built from lamellae. A bimodal character of the nanostructure is most clearly observed at high pressure and high molecular weight, where the scattering of an ensemble of thick lamellae is obvious in the vicinity of $s = 0$.

Interface distributions during UHMWPE heating as a function of molecular mass and molding pressure are shown in Figure 5. At the upper bound of the x axis (110 nm) almost all correlations among layers are faded away. During heating from room temperature to 100 °C, the dominant effect is a collective increase of all peak heights. It is caused from different thermal expansion coefficients of the amorphous and the crystalline domains.[31] This fact is reflected in the set of structural parameters extracted from the interface distributions, which show a considerable increase of the weight parameter as a function of temperature, whereas variation of the curve shape appears to be negligible.

Figure 6 shows some of the structural parameters as a function of temperature, molding pressure, and molecular mass. Indicated by error bars are the asymptotic intervals of confidence as computed by the nonlinear regression algorithm and as described previously.[29]

Solid lines are related to the lamellar stack component. The curves without symbol marks demonstrate the weight. As anticipated in the previous section, the weight shows an almost linear increase up to a temperature of 100 °C. At higher temperatures, weight decreases due to melting.

Filled squares show the average thickness of crystalline layers from the stack, $\bar{t}_{c,s}$. They can be identified from the fact that the relative widths of their distributions are considerably narrower than the relative widths of the amorphous layers. Moreover, at high temperature the amorphous distributions become very wide indicating transformation from stacks to uncorrelated crystalline lamellae. The average thickness of the crystalline lamellae is close to 20 nm. It is independent of molecular mass and molding pressure for all samples up to a
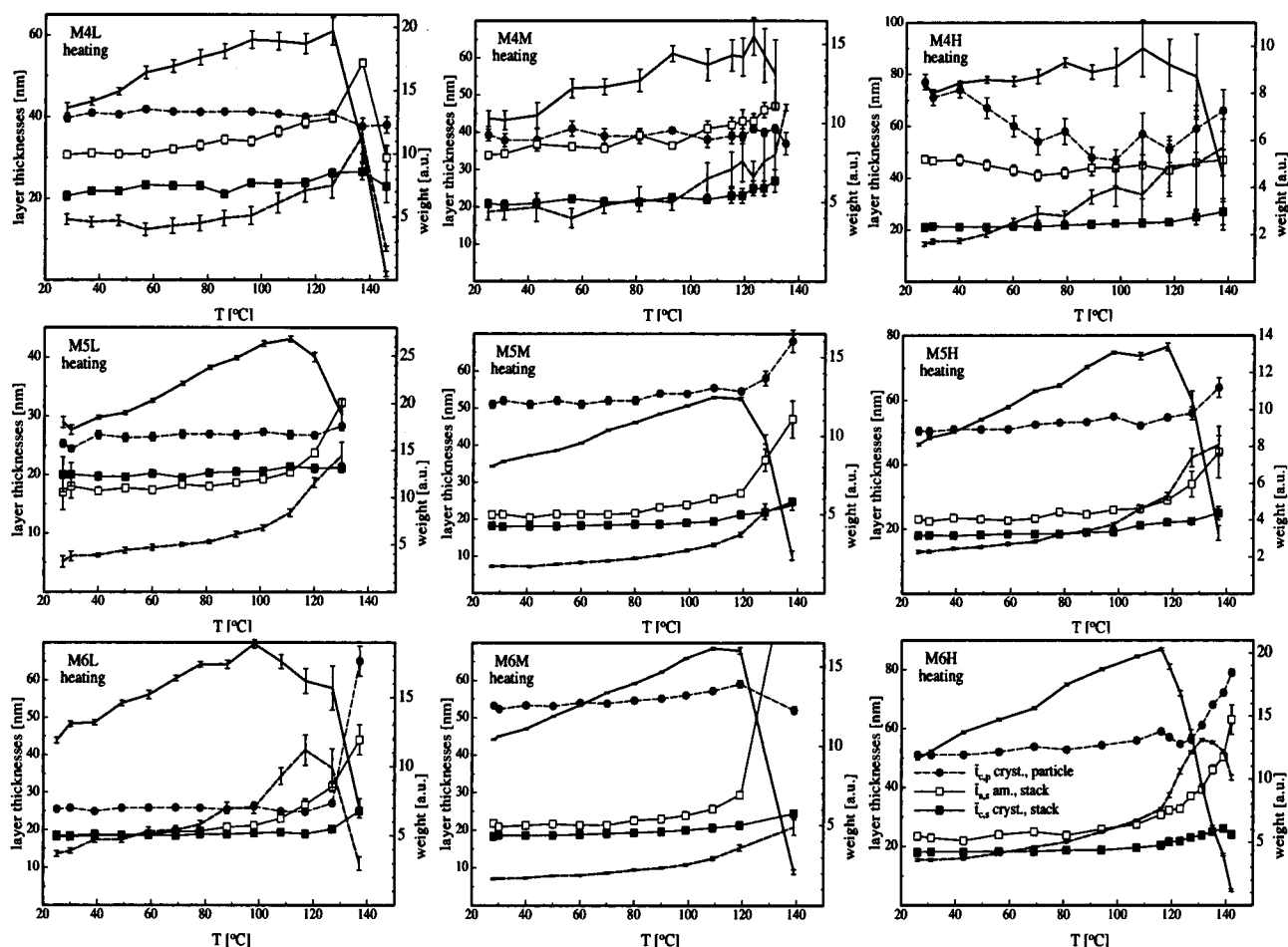
Figure 6. Nanostructure parameters from model fits of UHMWPE series during heating as determined from the IDFs. Curves without symbols show the weights W_i of components. Curves marked by symbols show layer thicknesses. Crystalline layers carry filled symbols. Solid lines: Stacks. Broken lines: Uncorrelated lamellae.

temperature of 120 °C. During subsequent melting a slight increase of the average value is observed.

Average amorphous layer thicknesses, $\bar{t}_{a,s}$, are marked by open squares. Up to a temperature of 100 °C, they are almost constant. As a function of increasing pressure a considerable increase of $\bar{t}_a$ is observed for all molecular masses. Linear crystallinity $v_{c,l} = \bar{t}_{c,s}/(\bar{t}_{c,s} + \bar{t}_{a,s})$ is smallest for the grade M4 with the lowest molecular mass (0.41 at low pressure, 0.30 at high pressure). The two grades M5 and M6 start with $v_{c,l} = 0.5$ at low pressure and end with 0.44 at high pressure. Thus crystallinity depression inside the stacks as a function of molding pressure is smaller for the grades M5 and M6.

The average layer thickness of the uncorrelated crystalline particles, $\bar{t}_{c,p}$, are shown by dashed curves marked with filled circles. Here the high molecular mass grades M5 and M6 are similar again. $\bar{t}_{c,p}$ remains constant up to 120 °C. It is 25 nm for low molding pressure and 50 nm for both medium and high molding pressures. Grade M4 is different. For low and medium molding pressures, we observe $\bar{t}_{c,p} = 40$ nm over a wide temperature range. The sample prepared at high molding pressure shows a linear decrease of $\bar{t}_{c,p}$ starting with 80 nm at room temperature and ending with 40 nm at 100 °C. As compared to the M5 and M6 grade, the layer thickness distributions are very wide, indicating imperfection. Even more imperfection can be concluded from the rapid joint collapse of both components in M4L at high temperature, observed in their weight curves. This

Table 1. Volume Fraction $V_{p,c}$ of Uncorrelated Crystalline Lamellae with Respect to the Total Volume of the Crystalline Phase as a Function of Molding Pressure and Molecular Mass of UHMWPE

	p		
	210 MPa	240 MPa	280 MPa
$M_w = 4 \times 10^6$ g/mol	0.37	0.31	0.42
$M_w = 5 \times 10^6$ g/mol	0.23	0.36	0.43
$M_w = 6 \times 10^6$ g/mol	0.28	0.31	0.46

is reflected in the feature of a single DSC melting peak of M4L (Figure 2).

Let us now discuss the effect of high molding pressure on the formation of thick crystalline lamellae, which is frequently addressed as "formation of extended chain lamellae".[26,32−37] Table 1 shows the volume fraction $V_{p,c}$ of uncorrelated, thick lamellar particles with respect to the total volume occupied by the crystalline phase at 30 °C as computed from eq 3. The high molecular weight grades M5 and M6 exhibit the frequently reported increase of the fraction of thick, uncorrelated lamellae as a function of increasing pressure. Again, the results of grade M4 can be explained by its imperfect nanostructure.

Figure 7 presents the variation of the crystalline volume, $xh_c(x)$, as a function of crystalline layer thickness x, temperature, molecular mass, and molding pressure. For low pressure (left column) the two populations of crystal layer thicknesses cannot be separated visually in the plots of M5L and M6L. Nevertheless,
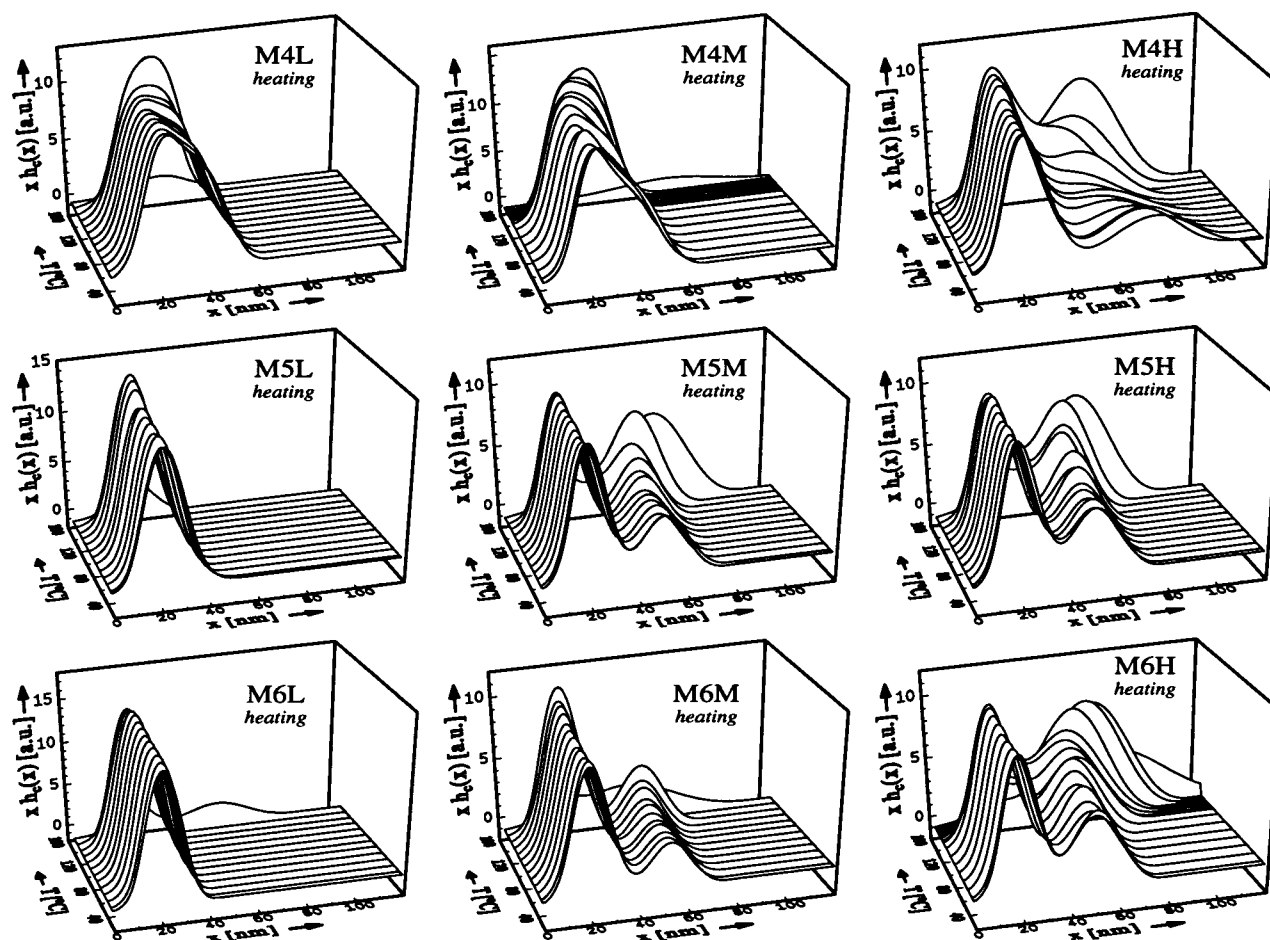
Figure 7. Crystalline volume $xh_c(x)$ as a function of lamella thickness x, temperature, molecular mass, and molding pressure during heating and melting of UHMWPE.

both DSC and quantitative SAXS data evaluations suggest that two populations should be present. The average layer thickness of the thick crystal lamellae is far below the thickness expected for fully extended chains. So it appears reasonable to assume that chain extension is imperfect. A different explanation would keep the notion of fully extended chains but change the chain orientation and put the chains parallel to the surface of the models "lamellae".

The samples from medium and high pressure clearly exhibit two crystalline layer thickness populations in the plots. In particular, for the high-pressure samples (right column), it becomes obvious that considerable amounts of "lamellae with chains seeking extension" are formed during the heating and after the crystal lamellae from the stacks start to melt. Thus USAXS reveals two processes coupled to each other, in which the melting of conventional crystalline layers initiates formation of thick lamellae. The DSC experiment shows that the net external heat flow of the superimposed processes is negligible. Only the subsequent melting of the thick crystal lamellae is observed in the thermogram.

However, even in the temperature regime between ambient temperature and 120 °C (before considerable amounts of the lamellae from the stacks start to melt), the USAXS experiment reveals the complexity of the dynamic process. The left drawing of Figure 8 presents the $xh_c(x)$ curves at 30 °C. In the right drawing, these curves are subtracted from the corresponding curves at 120 °C in order to visualize the total change of volume
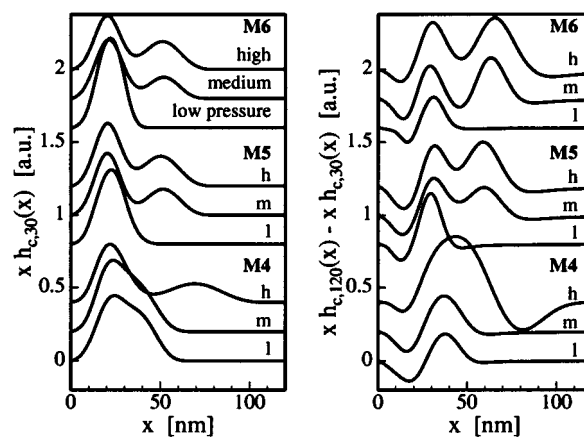

Figure 8. Melting of UHMWPE as a function of molecular mass and molding pressure. Left: (30 °C) $xh_c(x)$ is the volume filled with crystalline lamellae of thickness x. Right: Total change of $xh_c(x)$ after heating to 120 °C. Positive values denote crystallization; negative values stand for melting.

filled with crystal lamellae of thickness x. The drawing shows that, in general, heating to 120 °C causes the melting of lamellae which are thinner than approximately 30 nm, while crystallization occurs both in the stack component and in the ensemble of thick uncorrelated layers. Only with the unstable sample M4H is melting of imperfect thick lamellae observed. It should be mentioned that the apparent total crystallization observed in the right drawing is probably caused from

imperfect compensation of contrast increase as a function of temperature.

Conclusions

It has been shown that the time-resolved monitoring of the melting of several UHMWPE samples by the USAXS method results in substantial data, which can be described by a common principle nanostructural model from both thin crystal lamellae incorporated in stacks and thick layers which are placed at random. As a function of increasing molding pressure the fraction of thick layers is rising. These findings are consistent with common notion on the formation of extended chain lamellae.

It was observed that the melting of the thin crystal layers goes along with the formation of considerable amounts of extended chain crystals by crystallization. We may speculate that the original high-pressure injection-molded material is frozen in a nonequilibrium state and that crystals formed in a solidification process[25] prevent the material from adopting the equilibrium state. If this speculation holds, an annealing at a temperature between the melting of the chain-folded crystals and the melting of the extended-chain crystals could help to modify materials properties considerably.

Because melting is taking place in a relatively narrow temperature range, many images originate from a considerable interval what the variation of the nanostructure is concerned. Improvement of time resolution by a factor of 10 without being forced to sacrifice both data quality and the option to perform a quantitative analysis would greatly improve the obtainable results. Such improvement is becoming more important as the automated and quantitative evaluation of SAXS and USAXS data is advancing.

References and Notes

(1) Wang, Z.-G.; Hsiao, B. S.; Lopez, J.; Armistead, J. P. *J. Polym. Res.* **1999**, *6*, 167.
(2) Ruland, W. *Colloid Polym. Sci.* **1977**, *255*, 417.
(3) Fischer, L.; Haschberger, R.; Ziegeldorf, A.; Ruland, W. *Colloid Polym. Sci.* **1982**, *260*, 174.
(4) Fiedel, H. W.; Wenig, W. *Colloid Polym. Sci.* **1989**, *267*, 369.
(5) Santa Cruz, C.; Stribeck, N.; Zachmann, H. G.; Baltà Calleja, F. J. *Macromolecules* **1991**, *24*, 5980.
(6) Stribeck, N.; Zachmann, H. G.; Bayer, R. K.; Baltà Calleja, F. J. *J. Mater. Sci.* **1997**, *32*, 1639.
(7) Wolff, T.; Burger, C.; Ruland, W. *Macromolecules* **1994**, *27*, 3301.
(8) Stribeck, N.; Sapoundjieva, D.; Denchev, Z.; Apostolov, A. A.; Zachmann, H. G.; Stamm, M.; Fakirov, S. *Macromolecules* **1997**, *30*, 1329.
(9) Schmidtke, J.; Strobl, G.; Thurn-Albrecht, T. *Macromolecules* **1997**, *30*, 5804.
(10) Stribeck, N.; Reimers, C.; Ghioca, P.; Buzdugan, E. *J. Polym. Sci., Part B: Polym. Phys.* **1998**, *36*, 1423.
(11) Chen, H.-L.; Li, L.-J.; Lin, T.-L. *Macromolecules* **1998**, *31*, 2255.
(12) Thünemann, A. F.; Lochhaas, K. H. *Langmuir* **1998**, *14*, 6220.
(13) Heck, B.; Hugel, T.; Iijima, M.; Sadiku, E.; Strobl, G. *New J. Phys.* **1999**, *1*, 17.1.
(14) Stribeck, N. *ACS Symp. Ser.* **2000**, *739*, 41.
(15) Thünemann, A. F.; Ruland, W. *Macromolecules* **2000**, *33*, 2626.
(16) Iijima, M.; Strobl, G. *Macromolecules* **2000**, *33*, 5204.
(17) Wutz, C.; Stribeck, N.; Gieseler, D. *Colloid Polym. Sci.* **2000**, *278*, 1061.
(18) Heck, B.; Hugel, T.; Iijima, M.; Strobl, G. *Polymer* **2000**, *41*, 8839.
(19) Flores, A.; Pietkiewicz, D.; Stribeck, N.; Roslaniec, Z.; Baltá Calleja, F. J. *Macromolecules* **2001**, *34*, 8094.
(20) Fu, Q.; Heck, B.; Strobl, G.; Thomann, Y. *Macromolecules* **2001**, *34*, 2502.
(21) Hsiao, B. S.; Verma, R. K. *J. Synchrotron Radiat.* **1998**, *5*, 23.
(22) Hauser, G.; Schmidtke, J.; Strobl, G.; Thurn-Albrecht, T. *ACS Symp. Ser.* **2000**, *739*, 140.
(23) Hugel, T.; Strobl, G.; Thomann, R. *Acta Polym.* **1999**, *50*, 214.
(24) Stribeck, N. *Colloid Polym. Sci.* **2001**; in press.
(25) Dettenmaier, M.; Fischer, E. W.; Stamm, M. *Colloid Polym. Sci.* **1980**, *258*, 343.
(26) Wunderlich, B. *Macromolecular Physics*; Academic Press: New York, 1973; Vol. 1.
(27) Vonk, C. G.; Kortleve, G. *Kolloid-Z. Z. Polym.* **1967**, *220*, 19.
(28) Stribeck, N. *J. Appl. Crystallogr.* **2001**, *34*, 496.
(29) Stribeck, N. *Colloid Polym. Sci.* **1993**, *271*, 1007.
(30) Stribeck, N. *J. Phys. IV* **1993**, *3*, 507.
(31) Barnes, J. D.; Kolb, R.; Barnes, K.; Nakatani, A. I.; Hammouda, B. *J. Appl. Crystallogr.* **2000**, *33*, 758.
(32) Yasuniwa, M.; Yamaguchi, M.; Nakamura, A.; Tsubakihara, S. *Polym. J.* **1990**, *22*, 411.
(33) Baltá Calleja, F. J.; Öhm, O.; Bayer, R. K. *Polymer* **1994**, *35*, 4775.
(34) Hikosaka, M.; Amano, R.; Rastogi, S.; Keller, A. *Macromolecules* **1997**, *30*, 2067.
(35) Liangbin, L.; Pong, L.; Rui, H.; Wuyi, F.; Yunwei, L.; Hai, H. *J. Mater. Sci. Lett.* **1999**, *18*, 609.
(36) Flores, A.; Baltá Calleja, F. J.; Bassett, D. C. *J. Polym. Sci., Part B: Polym. Phys.* **1999**, *37*, 3151.
(37) Shcherbina, M. A.; Chvalun, S. N.; Aulov, V. A.; Selikhova, V. I.; Bakeev, N. F. *Polym. Sci., Ser. A* **2001**, *43*, 72.